JOURNAL OF NEUROTRAUMA 33:1834–1847 (October 15, 2016)

DOI: 10.1089/neu.2015.4239

White Matter Injury Susceptibility via Fiber Strain Evaluation Using Whole-Brain Tractography

Wei Zhao,[1] James C. Ford,[2] Laura A. Flashman,[2] Thomas W. McAllister,[3] and Songbai Ji[1,4]

Abstract

Microscale brain injury studies suggest axonal elongation as a potential mechanism for diffuse axonal injury (DAI). Recent studies have begun to incorporate white matter (WM) structural anisotropy in injury analysis, with initial evidence suggesting improved injury prediction performance. In this study, we further develop a tractography-based approach to analyze fiber strains along the entire lengths of fibers from voxel- or anatomically constrained whole-brain tractography. This technique potentially extends previous element- or voxel-based methods that instead utilize WM fiber orientations averaged from typically coarse elements or voxels. Perhaps more importantly, incorporating tractography-based axonal structural information enables assessment of the overall injury risks to functionally important neural pathways and the anatomical regions they connect, which is not possible with previous methods. A DAI susceptibility index was also established to quantify voxel-wise WM local structural integrity and tract-wise damage of individual neural pathways. This ''graded'' injury susceptibility potentially extends the commonly employed treatment of injury as a simple binary condition. As an illustration, we evaluate the DAI susceptibilities of WM voxels and transcallosal fiber tracts in three idealized head impacts. Findings suggest the potential importance of the tractography-based approach for injury prediction. These efforts may enable future studies to correlate WM mechanical responses with neuroimaging, cognitive alteration, and concussion, and to reveal the relative vulnerabilities of neural pathways and identify the most vulnerable ones in real-world head impacts.

Key words: Dartmouth Head Injury Model; fiber strain; neural pathway; tractography; traumatic brain injury; white matter injury

Introduction

Traumatic brain injury (TBI) is a leading cause of morbidity and mortality in the United States.[1] To better understand the mechanisms of brain injury at the macroscale level, numerous kinematic injury metrics have been proposed (e.g., peak linear [a_{lin}] and/or rotational [a_{rot}] accelerations, or their derivatives such as Head Injury Criterion [HIC],[2] Rotational Injury Criterion [RIC] and Power Rotational Head Injury Criterion [PRHIC],[3] Brain Injury Criteria [BrIC],[4] Generalized Acceleration Model for Brain Injury Threshold [GAMBIT],[5] Head Impact Poser [HIP],[6] and the HIT severity index[7]). Unfortunately, they are not directly related to the brain mechanical responses believed to initiate the injury,[8] and as of yet, no consensus has been reached on an appropriate injury metric or a threshold to date. Further, these metrics have been shown to be less effective in injury prediction than brain mechanical responses estimated from validated finite element (FE) models.[3,9–11]

Most of the model-based injury studies use isotropic response variables, such as the maximum principal strain (ε_{ep}), that are not capable of characterizing white matter (WM) axonal shearing[12,13] or elongation,[14,15] both of which have been thought to cause morphological injury and functional impairment in diffuse axonal injury (DAI) at the microscale level. To address this inconsistency, recent studies have begun to use strains along WM fibers to characterize elongation of axonal bundles (termed ''axonal'' or ''fiber'' strain, ε_n).[11,16–22] Initial evidence suggests that fiber orientation-dependent ε_n improves injury prediction relative to its isotropic counterpart, ε_{ep}.[11,18,21,22]

Ji and colleagues[22] used subject-specific head FE models to evaluate and compare ε_n with ε_{ep} for a group of 11 athletes with concussion.[22] They found that the two strain measures differed significantly in distribution and extent of WM exposure to high strains. Further, the distribution of WM regions with high ε_n was consistent with typical heterogeneous patterns of WM disruptions

[1]Thayer School of Engineering, Dartmouth College, Hanover, New Hampshire.
[2]Department of Psychiatry, Geisel School of Medicine at Dartmouth, Lebanon, New Hampshire.
[3]Department of Psychiatry, Indiana University School of Medicine, Indianapolis, Indiana.
[4]Department of Surgery and of Orthopaedic Surgery, Geisel School of Medicine at Dartmouth, Lebanon, New Hampshire.

in DAI. On a group-basis, the average extent of WM injury assessed at an optimal strain threshold also matched well with the percentage of WM voxels experiencing significant longitudinal changes in fractional anisotropy (FA) and mean diffusivity found from another independent imaging study.[23] These findings were supported by the work from Giordano and Kleiven,[11] who studied 58 National Football League sports accidents and concluded that ε_n performed better in injury prediction than ε_{ep}, CSDM (Cumulative Strain Damage Measure based on ε_{ep}[24]), BrIC, or HIC.

While these studies suggest the importance of WM structural anisotropy,[25] continued development along this line of research by incorporating whole-brain tractography derived from diffusion tensor imaging (DTI) for ε_n evaluation may improve the injury prediction performance even further. The reason is that tractography potentially allows more accurate estimation of fiber orientations at each individual high resolution sampling point (e.g., every 1 mm along fibers or ''streamlines'') than those ''averaged'' at coarse FE elements or voxels (e.g., element size up to 7.73 mm,[26] or DTI voxel size of 2 mm ×2 mm ×3.6 mm[27]).

For example, Chatelin and associates[18] used weighted directions averaged from 70–4096 DTI voxels for each element. Both Cloots and coworkers[17] and Wright and Ramesh[19] employed a multiscale approach to couple a macroscale three dimensional (3D) or two dimensional (2D) head model, respectively, with a microscale element embedding a single axon. Work from Wright and colleagues,[21] Kraft and associates,[20] Sahoo and coworkers,[26], and Giordano and Kleiven[27] assigned average FA values and fiber directions to each element from coregistered DTI for strain evaluation. Instead of averaging on elements, Ji and associates[22] evaluated fiber strain at each DTI voxel transformed into the corresponding FE model space using strain tensors from the closest FE element on a subject-specific basis.

Assessing tractography-based fiber strains is of particular interest in WM regions with crossing fibers or other complex fiber configurations. In addition, the ability to evaluate ε_n at a finer spatial resolution also enables assessing WM voxel-wise injury vulnerabilities at a scale finer than a simple injured versus non-injured binary status, as is commonly used. Perhaps more importantly, analyzing strains along the entire lengths of fibers enables assessing the injury risks to WM neural pathways or tracts, which is not possible with previous element/voxel-based studies that are limited to anatomical regions of interest (ROIs). Because axons and their bundles are neural processes that connect neuronal cell bodies and transmit information between them,[28,29] it is reasonable to assume that any damage along the axons, regardless of the location (within or outside the boundary of any traversing ROI), would constitute potential functional impairment.[20]

The goal of this study was to develop a technique to evaluate ε_n along voxel- or anatomically constrained whole-brain tractography, which has not been performed before. An ''injury susceptibility index'' was developed to quantify injury vulnerabilities with a finer, graded ''likelihood'' of injury of discrete WM voxels or individual neural pathways, extending previous efforts where typically a dichotomous injury status was instead assigned. As an initial step, here we focus our efforts on comparing the new tractography-based method and our previous voxel-based technique for fiber strain analysis using idealized head rotations.

As an illustration, we investigated the injury susceptibilities of the whole-brain WM voxels as well as transcallosal fiber tracts traversing the corpus callosum (CC). Finally, these efforts allowed us to investigate the ε_n response's directional sensitivity. If ε_n is indeed a more effective injury predictor, our investigation using a realistic 3D model incorporating whole-brain tractography is a significant advancement over previous studies using 2D head models coupled with projections of fiber directions [21] or those based on ε_{ep}.[30–32] Collectively, these efforts extend our previous investigations[22,33,34] and set the stage for future studies to explore the causal relationships among brain mechanical responses, WM structural integrity, and brain functional alteration or clinical symptomatic measures in subjects with TBI.

Methods

The Dartmouth Head Injury Model

All brain strain responses were obtained using the Dartmouth Head Injury Model (DHIM; Fig. 1). The DHIM is a subject-specific model created with high mesh quality and geometrical accuracy based on high-resolution magnetic resonance imaging (MRI) of an athlete. Details of the model description, material properties, and validation performances were reported previously.[22,35,36]

Briefly, the DHIM is composed of solid hexahedral and surface quadrilateral elements with a total of 101.4 k nodes and 115.2 k

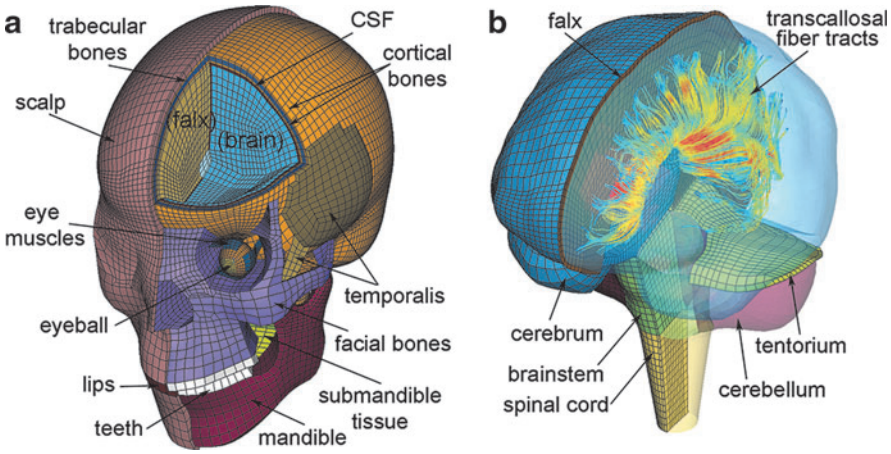

FIG. 1. The Dartmouth Head Injury Model (DHIM) showing the head exterior (**a**) and the brain components (**b**). The model incorporates whole-brain tractography from the same individual used for the baseline DHIM creation. A subset of fractional anisotropy-encoded transcallosal fibers is shown (b). CSF, cerebrospinal fluid. Color image is available online at www.liebertpub.com/neu

elements and a combined mass of 4.562 kg for the whole head. The brain has a total of 56.6 k nodes and 55.1 k elements, with a combined mass of 1.558 kg. The average element sizes for the whole head and the brain are 3.2 ± 0.94 mm and 3.3 ± 0.79 mm, respectively.

The entire brain is modeled with the C3D8R type of hexahedral elements[37] using a homogenous, second-order Ogden hyperelastic material model with rate effects incorporated through linear viscoelasticity. A layer of soft elements representing the cerebrospinal fluid between the brain and its neighboring structures (skull, falx, and tentorium) is incorporated by node sharing to enable brain interfacial sliding.

The DHIM has successfully passed the numerical convergence test and is of high mesh quality in terms of warpage, aspect ratio, skew, Jacobian, minimum length, and minimum/maximum angle.[22] In addition, the model has been successfully validated against relative brain-skull displacement[38,39] and intracranial pressure responses[40,41] from cadaveric experiments, as well as full-field strain responses in a live human volunteer.[42] The overall ''good'' to ''excellent'' validation at the low ($\sim$250–300 rad/s^2 for the volunteer), mid ($\sim$1.9–2.3 krad/s^2 for impact tests C755-T2 and C383-T1), and high ($\sim$11.9 krad/s^2 for test C393-T4) levels of a_{rot} peak magnitudes as well as pressure responses provided important confidence of the accuracy of DHIM-estimated brain responses. In this study, the high-resolution T1-weighted MRI and DTI of the same individual used to develop the baseline DHIM were used for image registration, tractography, and strain computation.

Neuroimage acquisition

T1-weighted MRI (Magnetization Prepared Rapid Gradient Echo, MPRAGE; voxel resolution of 1.2 mm $\times$1 mm $\times$1 mm) and DTI (isotropic resolution of 2 mm) scans were acquired in the Dartmouth Advanced Imaging Center. DTIs had 46 diffusion directions (collected with b = 1000 s/mm^2, NEX = 1) plus an additional volume without diffusion gradients (b = 0) serving as a reference image. Diffusion tensors, eigenvectors, and scalar diffusion parameters were computed using a well-established tractography software package, ExploreDTI,[43] with corrections for eddy currents and motion before fitting a tensor model.

In this study, we used the pre-season DTI scans of the selected person to generate whole-brain tractography via ExploreDTI using the default set of parameters for a deterministic streamline approach, which were selected for optimized performance.[43] Tracts were propagated from all brain voxels as seed points following the direction of the principal diffusion orientation at each seed point and subsequent voxel with a 1 mm step size and linear interpolation. Tracts were terminated if FA fell below a specified threshold (0.2) or if the tract angle changed by more than 30 degrees. All tracts with lengths of 50 to 500 mm were retained, resulting in $\sim$35 k fibers for the selected individual.

Voxel- and anatomically constrained fiber tract clustering

Intravoxel fibers traversing a given voxel were identified from the whole-brain tractography by testing whether any fiber sampling point fell inside the boundary of the corresponding hexahedral element converted from the voxel. Automatic clustering of fiber tracts/bundles based on anatomical ROIs is still an active, ongoing research topic. Here, we adopted an existing method[44] to identify transcallosal fibers using the ICBM DTI-81 WM atlas[45] as an anatomical constraint. This atlas is a stereotaxic probabilistic map averaged from 81 normal subjects with hand-segmented WM parcellation of 50 deep WM structures. The atlas is provided within a standard anatomical template (ICBM-152, isotropic image resolution of 1 mm[45]), which allows for transformation of a given individual's MRI and WM atlas into the same coordinates via affine registration. The registration was performed between the MPRAGE MRI of the individual selected for DHIM creation and the ICBM-152 template, using the ITK Segmentation and Registration Toolkit (Version 4.7; Fig. 2).

Transcallosal fibers from the whole-brain tractography were identified by testing whether they traversed the genu, splenium, or main body of the CC based on the ICBM DTI-81 WM atlas. This could be determined by first transforming the fiber sampling points into the WM atlas space and then rounding their coordinates to their closest voxels to perform a voxel-wise overlapping test.[44] Alternatively, we converted CC voxels into hexahedral elements instead and directly tested whether real-valued coordinates of fiber sampling points fell inside the outer boundary of the aggregated hexahedral mesh. This avoided rounding errors and reduced the number of spuriously intersecting fibers.

To further minimize ''outlier'' fibers spuriously intersecting the target region, thresholding was performed based on the number of intersection points.[44] Additional filtering based on geometry and tract self-consistency was also performed (e.g., by fitting each fiber into a plane to test its orientation, or by assessing the average distance from fiber sampling point relative to the tract centroid). For each CC subregion, less than 3% of the total number of fibers were considered spurious and were thus removed. This led to 1740, 2866, and 2661 fibers retained for the genu, splenium, and main body of the CC, respectively. The clustering process is illustrated in Figure 3.

Idealized head impacts

Brain responses corresponding to axial, coronal, and sagittal (anterior-to-posterior) rotations (Fig. 4a) were selected from an existing pre-computed brain response atlas (pcBRA[32,46]). The pcBRA employs triangulated a_{rot} impulses applied to the head center of gravity (skull, scalp, and facial components were simplified as rigid bodies). The shape of the acceleration impulse is not important (e.g., triangular, sine, or haversine), as long as the peak rotational velocity and impulse duration remain identical.[46]

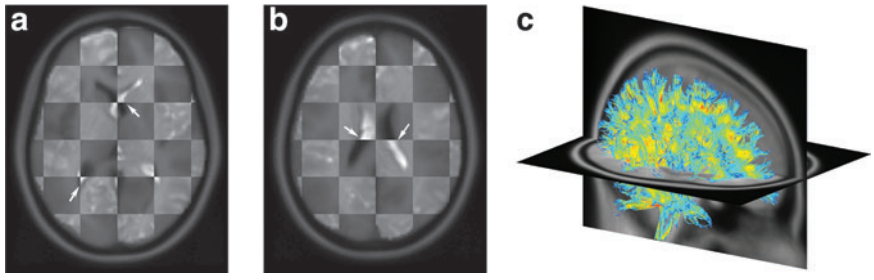

FIG. 2. Checkerboard images overlaying the individual's magnetic resonance image (appears lighter) with the coregistered ICBM-152 template (background; appears darker) on two axial planes (**a,b**). The alignment (arrows) suggests a satisfactory registration. A 10% randomly selected subset of the individual's fractional anisotropy-encoded, whole-brain tractography is shown in the ICBM-152 space (**c**). Color image is available online at www.liebertpub.com/neu

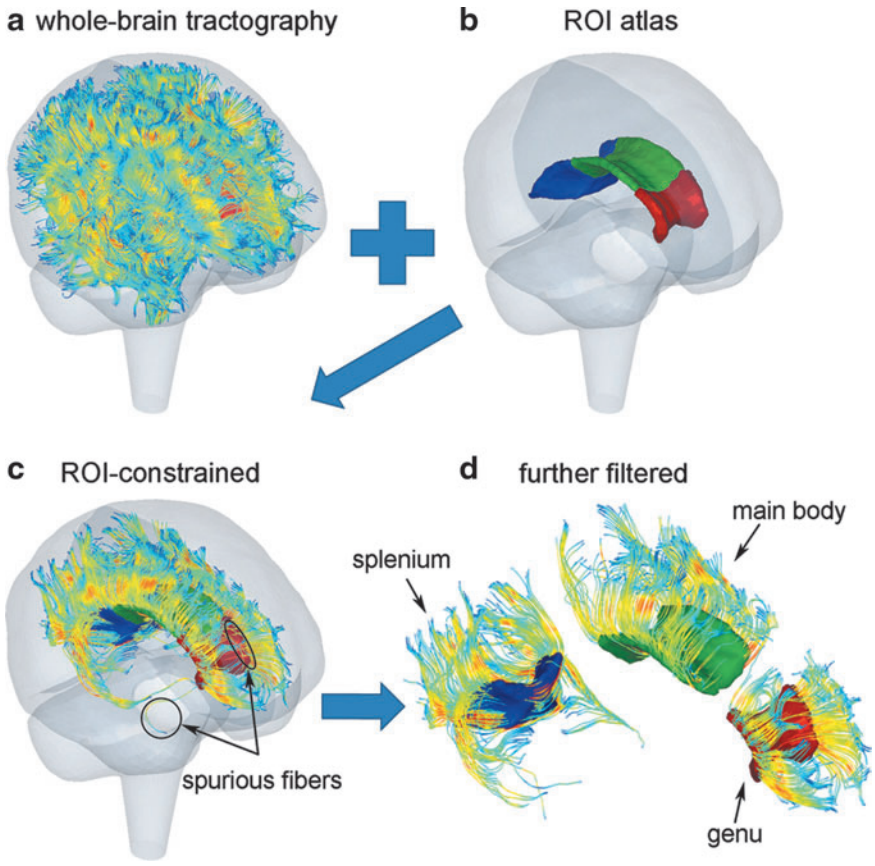

FIG. 3. Illustration of anatomically or region of interest (ROI) constrained fiber tract clustering. (**a**) Fractional anisotropy-encoded whole-brain tractography overlaid within the Dartmouth Head Injury Model brain mesh boundary; (**b**) anatomical boundaries of the three corpus callosum subregions; (**c**) the resulting ROI-constrained transcallosal fiber tracts; (**d**) spurious fibers further filtered. A 10% randomly selected fiber sample is shown. Color image is available online at www.liebertpub.com/neu

For the selected brain responses, the a_{rot} impulse had a peak magnitude of 4.5 krad/s^2, which was the 95th percentile of all measured a_{rot} peak magnitudes observed in collegiate ice-hockey (concussed and nonconcussed[47]) and was slightly below the median or average a_{rot} peak magnitudes for concussive impacts measured in collegiate football.[48] The impulse duration was 10 msec (average value for a_{lin} found in high-school football[49]; report on typical duration for a_{rot} unavailable). The total simulation time was 28 msec with a temporal resolution of 1 msec, which was composed of a 10 msec acceleration impulse plus an additional 18 ms ''hold'' with zero a_{rot} (i.e., at a constant rotational velocity) to ensure peak responses were captured (Fig. 4b).

The choice of this particular acceleration-only profile without deceleration was made to mimic actual on-field head impact data available, where a single largest acceleration peak dominates.[50,51] Linear acceleration, a_{lin}, was not used here because a_{lin} -induced brain strain responses are negligible because of the near incompressibility of the brain. This was confirmed in terms of both maximum principal strain, ε_{ep} (using DHIM and an independently developed head model, SIMon[36]), and WM fiber strain, $\varepsilon_{n.}$.[21]

Injury susceptibility index

For each WM DTI voxel, the accumulated peak ε_n, regardless of the time of occurrence, ε_n^p, was computed for all its enclosing sampling points based on the Lagrangian strain tensor.[22] Each sampling point was considered ''injured'' when its ε_n^p exceeded a given threshold, ε_{thresh}. A voxel-wise injury susceptibility index, φ_{voxel}, was defined as the fraction of ''injured'' sampling points within the voxel, or formally:

$$\varphi_{voxel}(\varepsilon_{thresh}) = \frac{\#\ of\ injured\ sampling\ points\ within\ the\ voxel}{total\ \#\ of\ sampling\ points\ within\ the\ voxel}. \quad (1)$$

The value of φ_{voxel} in percentage ranges from 0% (no injury) to 100% (fully damaged).

Quantifying WM structural integrity or the ''likelihood'' of injury locally at each voxel is important to correlate brain mechanical responses with neuroimaging at the voxel level. Nonetheless, it does not capture the degree of functional impairment of a neural pathway, which could be of interest for clinical symptomatic measures. Here, we considered an anatomically constrained fiber (i.e., a single streamline in tractography passing through a given ROI) as injured when at least one sampling point, regardless of the location — either within or outside the ROI boundary—has ε_n^p exceeding ε_{thresh}. This is important, because global functional impairment of a fiber could occur regardless of the injury location. A tract-wise injury susceptibility index (φ_{tract}) was therefore analogously defined as the fraction of injured fibers from the entire tract:

$$\varphi_{tract}(\varepsilon_{thresh}) = \frac{\#\ of\ injured\ fibers\ for\ the\ given\ neural\ tract}{total\ \#\ of\ fibers\ for\ the\ given\ neural\ tract}. \quad (2)$$

The injury susceptibility indices depend on a pre-defined injury threshold. For illustration purposes, here we selected two representative ε_{thresh} values (0.18 and 0.09, corresponding to the upper and lower bounds of a conservative threshold; the former is also an

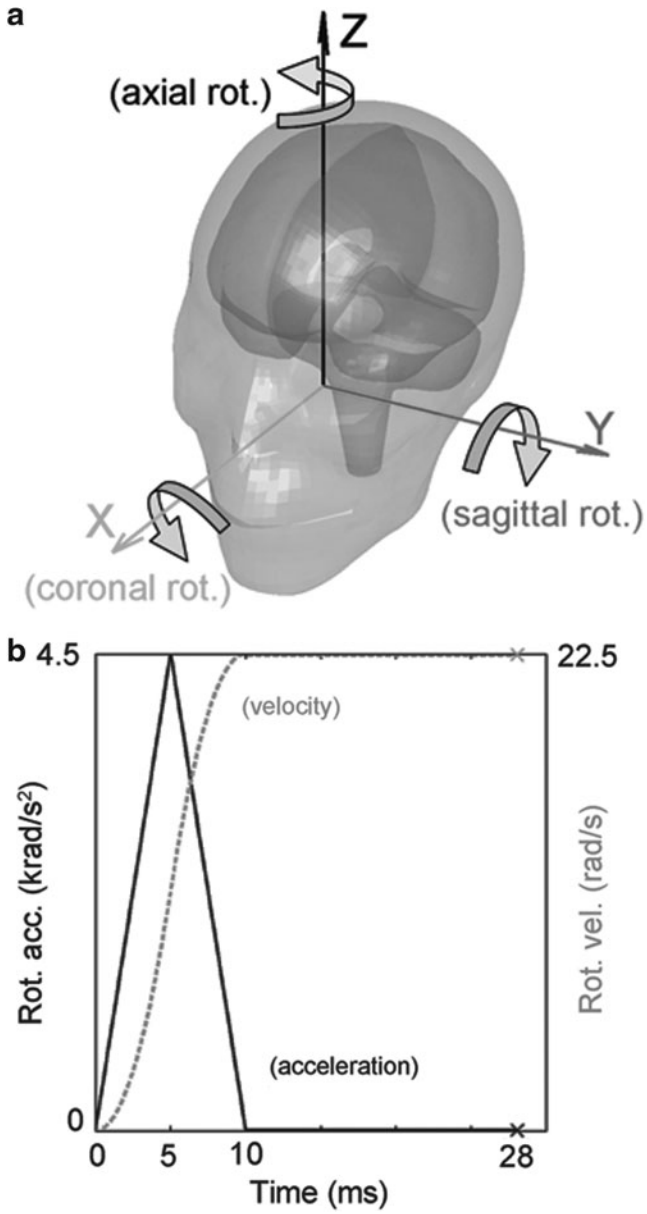

FIG. 4. Illustration of the three idealized head rotations (**a**) and the acceleration/velocity profile used for impact simulation (**b**).

''optimal'' threshold[14]) to create injury susceptibility maps based on the voxel-wise average ε_n^p. While these injury thresholds drawn from an *in vivo* animal study do not apply directly to the human brain, the optimal value was comparable to thresholds established from other real-world injury analyses in human TBI studies (albeit, based on ε_{ep} ; e.g., 0.21 in the CC or 0.26 in the gray matter, or 0.19 in the gray matter[52,53]). The lower bound value was also selected here because it was likely relevant to subconcussive impacts to the brain (which most likely correspond to a lower threshold).

Strategies to assess tract-wise injury susceptibility

Effectively, φ_{tract} incorporates the axonal structural information to evaluate injury susceptibilities of WM neural tracts. Current model-based studies, however, typically assess the degree of injury based on an aggregated volume fraction of the whole-brain or specific anatomical ROIs exceeding a threshold, regardless of the location or distribution of high strain exposures.[3,4,31,54] Therefore, we further compared φ_{tract} with injury susceptibility measures based on the number or ''fraction'' of all sampling points as well as all traversing WM voxels for a given tract, regardless of whether injury occurred along the same or different fibers. Two additional injury susceptibility measures are defined, analogously to the CSDM[24] but applied to a neural tract:

$$\varphi_{tract}^{point}(\varepsilon_{thresh}) = \frac{\#\ of\ injured\ sampling\ points\ for\ the\ tract}{total\ \#\ of\ sampling\ points\ for\ the\ tract}, \quad (3)$$

and

$$\varphi_{tract}^{voxel}(\varepsilon_{thresh}) = \frac{\#\ of\ injured\ traversing\ WM\ voxels}{total\ \#\ of\ traversing\ WM\ voxels\ for\ the\ tract}. \quad (4)$$

The different WM injury susceptibility indices are illustrated in Figure 5.

Data analysis

Voxel-wise binary injury maps were created by considering voxels with $\varphi_{voxel} > 50\%$ as ''injured'' (i.e., chosen as the mean value of φ_{voxel} corresponding to no injury (0%) and full damage [100%]). Similarly, binary injury maps based on averaged fiber orientations were also produced using the previous voxel-based approach.[22] The two injury maps were then compared in terms of predicted WM injury percentages and Dice coefficient (d) to assess the extent of injury and consistency in injury distribution, respectively. The Dice coefficient was previously used to compare predicted injury distributions using ε_n^p and the corresponding accumulated peak ε_{ep}, ε_{ep}^p.[22]

For the three transcallosal fiber tracts, distributions of ε_n^p were generated for comparison. The tract-wise injury susceptibility index, φ_{tract}, and the resulting binary ''injury'' prediction depend on ε_{thresh} (Eqn. 1). A definitive ε_{thresh} for the human brain has not been established, however. Therefore, we parametrically varied ε_{thresh} across a range of values (range 0–0.25, with a step size of 0.0025) to create ε_{thresh}-dependent functions to gain insight into its significance for φ_{tract}. Further, we compared φ_{tract} with φ_{tract}^{point} and φ_{tract}^{voxel}.

The computational time to obtain ε_n^p for all WM voxels (N = 64.3 k) for a 28 msec impact simulation using the voxel- and tractography-based approach was ~12 min and ~66 min, respectively. The time to obtain ε_n^p along the transcallosal fiber tracts (total of 7267 fibers with 813.2 k sampling points) was ~28 min, which scaled approximately linearly when compared with running on a 10% subset. All data analyses were performed with in-house programs (not yet optimized) in MATLAB (R2014a; MathWorks, Natick, MA) on a 12-core Linux machine (Intel Xeon X5560, 2.80 GHz, 126 GB memory).

Results

The voxel- and tractography-based approaches produced largely similar distribution patterns for real-valued ε_n^p for the three idealized impacts (Pearson correlation coefficient of 0.92, 0.91, and 0.90 for the axial, coronal, and sagittal rotation, respectively, with $p = 0$; Fig. 6). Not surprisingly, the latter produced smoother distributions because more sampling points were used to compute an average ε_n^p for each voxel (vs. effectively only one with the former). The corresponding maps of φ_{voxel} (0.09) are also shown.

The tractography-based binary or dichotomous injury maps (thresholded from real-valued ε_n^p maps in Fig. 6) were compared against those generated from the voxel-based approach (Fig. 7). The two ε_n^p evaluation techniques produced discordant distributions of voxels susceptible to injury, especially when ε_{thresh} was high (the average Dice coefficient, d, dropped from 0.81 to 0.66 when ε_{thresh} increased from 0.09 to 0.18; Table 1). For all injured voxels

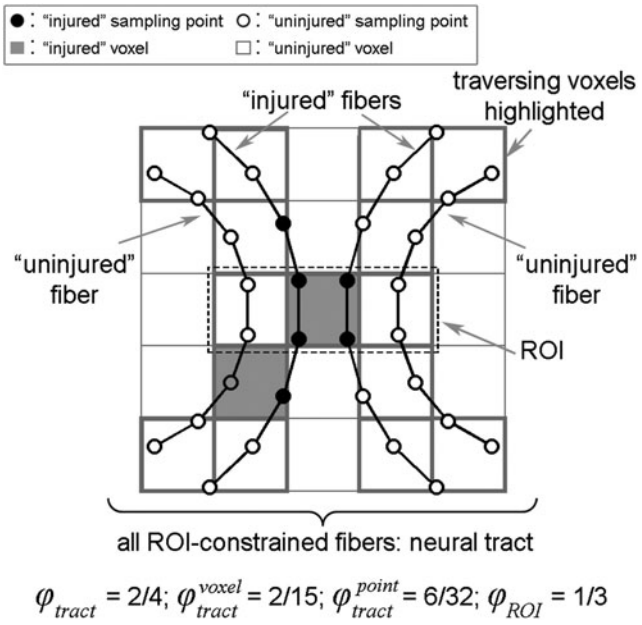

FIG. 5. Illustration the different injury susceptibility indices (see text for details). ROI, region of interest.

predicted by at least one approach, one-tailed two-sample *t* tests indicated that voxels consistently predicted as injured by both techniques had a significantly higher mean FA value than those predicted by only one method, regardless of ε_{thresh} or rotational direction ($p < 0.01$; Table 1). Interestingly, both approaches predicted a comparable extent of potential injury for the whole-brain WM voxels, or proportion of CC subregions affected, regardless of ε_{thresh} or rotational direction (Table 2).

To further compare the two strain evaluation approaches, three representative voxels in the axial rotation were selected that were either consistently predicted as potentially injured by both techniques or by one but not the other (Fig. 8). Their ε_n response histories are shown (Fig. 8b). When intravoxel fibers were highly aligned (corresponding to a high FA value for the voxel; Fig. 8c), ε_n^p responses varied smoothly across the sampling points. Heterogeneity and discontinuity were evident when otherwise (Fig. 8d and e).

For the range of ε_{thresh} values, φ_{tract} was computed for each CC subregion and head impact (Fig. 9). Consistent with the distributions of real-valued ε_n^p (Fig. 6) and thresholded, binary-valued injury locations (Fig. 7), the axial and sagittal rotations appeared the most and least damaging, respectively, in terms of the number of voxels with high ε_n^p exposures. The relative vulnerabilities of the three CC subregions, however, depended on the direction of head rotation (e.g., the genu was the most vulnerable in an axial rotation, but was the least in the other two rotations). The relative vulnerabilities were similarly observed using φ_{tract}^{point} and φ_{tract}^{voxel} that employed the aggregated numbers of injured sampling points and voxels, respectively (Fig. 10). They were significantly lower, however, than the corresponding φ_{tract} based on the injured fibers that incorporates WM axonal structural information.

Discussion

Recent brain injury studies suggest the importance of incorporating WM structural anisotropy for improved injury prediction performance.[25] Here, we extended previous work that used average orientations on coarse elements[18,20,21,27] or voxels[22] to analyze accumulated peak fiber strain, ε_n^p, along the entire lengths of fibers using whole-brain tractography. Each fiber was represented by high resolution (1 mm) sampling points, improving on the native DTI voxel resolution (2 mm). More importantly, a tractography-based analysis allowed assessment of injury vulnerabilities of entire WM neural pathways, which is not possible with previous ROI-based methods.

Assessing the mechanical responses of functionally important WM neural pathways may be of particular interest for future studies that correlate them with subtle changes in cognition for brains with or even without clinically diagnosed concussion.[33,55] As an initial illustration, we have demonstrated this tractography-based technique using idealized head impacts in the context of sports-related concussion for all WM voxels as well as three transcallosal fiber tracts, with results compared with those from a voxel-based approach.

At the voxel level, a unique capability of our tractography-based technique that appears unachievable with an element/voxel-based analogue was to enable assessment of the ''degree'' (vs. dichotomy) of WM structural damage. This was quantified in terms of a voxel-wise injury susceptibility index (φ_{voxel}), which is essentially the proportion of ''injured'' intravoxel sampling points.

This ''graded'' susceptibility (vs. a binary injury status) may provide a confidence measure in injury definition. For example, it could serve as a voxel selection criterion when comparing brain mechanical responses with longitudinal neuroimaging alterations (e.g., larger φ_{voxel} values indicate higher likelihood of injury). Potentially, this concept may be further extended to an anatomical ROI, in which case a φ_{ROI} can be analogously defined to characterize a regional injury susceptibility (Fig. 5). Such voxel-wise or ROI-based utilities await further exploration.

Interestingly, with an empirical injury susceptibility threshold of 50% to define a binary injury, the tractography-based approach predicted an extent of WM injury (i.e., volume fraction or number of injured voxels) comparable to that from the voxel-based technique for all cases evaluated (Table 2). This finding suggests a certain fundamental concordance between the two approaches. For a ''binary'' injury prediction based on the volume or number of injured WM voxels for the whole-brain, a DTI voxel-based method appears sufficient and may be preferred because of its relatively modest computation relative to the tractography-based analogue ($\sim$12 min vs. $\sim$66 min in this work).

The two approaches can differ significantly, however, in terms of binary injury distribution after thresholding (despite the similar pattern of real-valued ε_n^p maps; Fig. 6), especially in regions with low FA values or at a high ε_{thresh}, as evidenced by Dice coefficients (Table 1). These observations suggest further studies using real-world injury cases are required to discern the relative injury predictive power of the two competing strain evaluation techniques, e.g., by correlating injury predictions with voxel-wise neuroimaging findings.[23,56]

Regardless, another unique capability of our tractography-based technique is to assess injury susceptibilities for functionally important WM neural pathways, which does not appear feasible with a voxel-based approach. Because fibers serve as communication connections between functionally important cortical areas, injury assessment along their entire lengths (vs. confined within an ROI boundary) is likely critical to capturing the overall vulnerability of a given neural pathway. This is illustrated in Figure 8a (arrow), where potential injury locations with high ε_n^p exposures occurred outside the anatomical boundary of the CC,

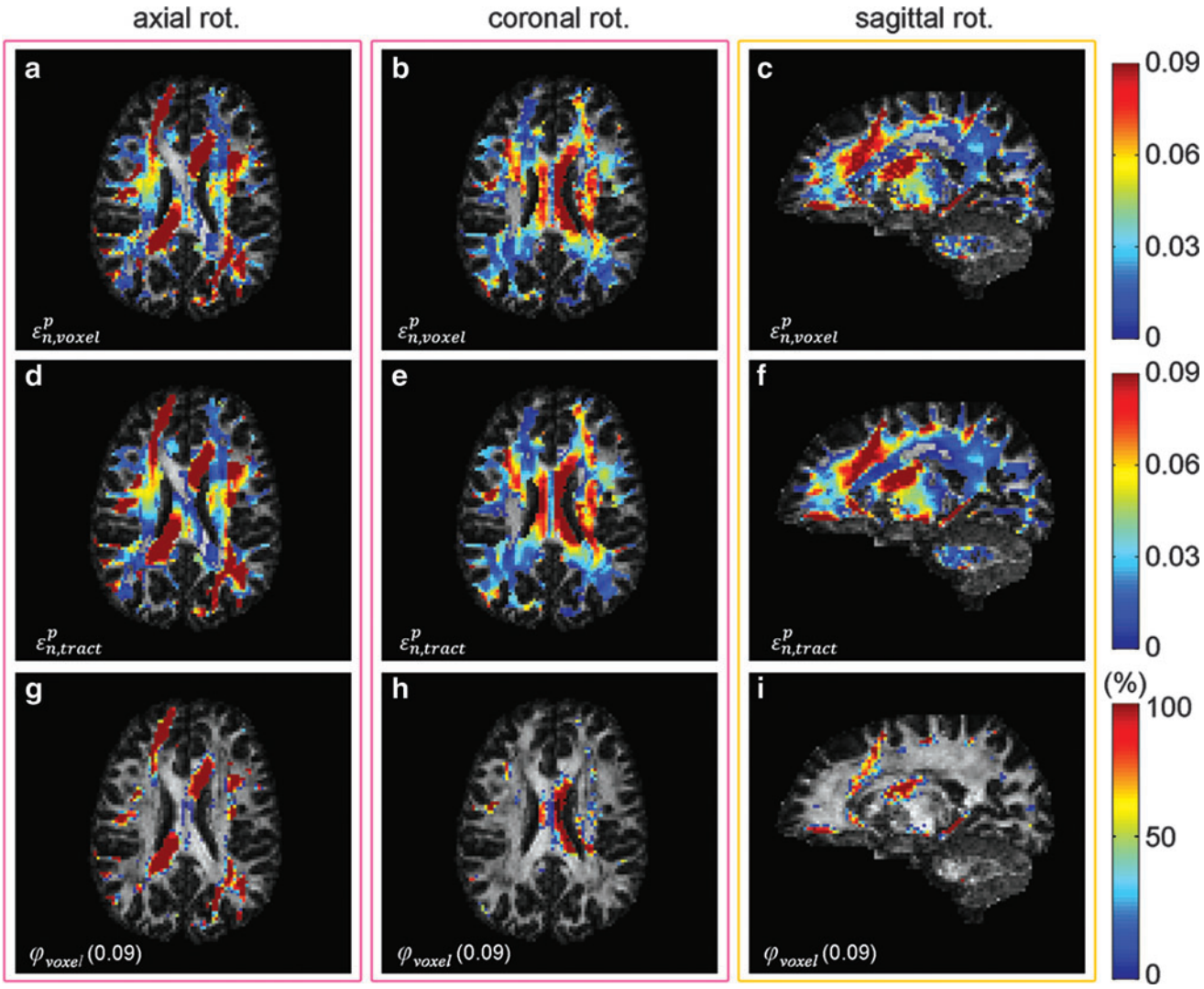

FIG. 6. Maps of ε_n^p using the voxel- (top) and tractography-based (middle row) approaches, along with the injury susceptibility maps (bottom) on a selected axial or sagittal magnetic resonance image in axial, coronal, and sagittal rotation (from left to right, respectively). Color image is available online at www.liebertpub.com/neu

but in tracts directly linked to it. This finding suggests that previous region-based, element-/voxel-wise injury studies may not be able to capture the overall vulnerability of ROI-associated WM neural pathways, which are important structural substrates to brain function.

The degree of damage to neural tracts can be similarly assessed with a tract-wise injury susceptibility index, which is essentially the proportion of potentially injured fibers, a measure intended to approximate that of ''injured'' axons.[57] As an illustration, we computed φ_{tract} based on ε_n^p for the three major transcallosal fiber clusters traversing the genu, splenium, and main body of the CC. Results from a 10% subset of fibers were virtually identical to that from the full set for all cases evaluated regardless of ε_{thresh} (a linear fit of φ_{tract} between the two sets led to a Pearson correlation coefficient of 0.99 for the pooled data, not shown; Fig. 9).

The feasibility to down-sample while preserving φ_{tract} is important, because fibers from tractography themselves are effectively a representative approximation of the actual whole-brain axons. Further, reduced computational cost is an important practical benefit. Excessive down-sampling should be avoided, however, as insufficient sampling may cause φ_{tract} to become unreliable.

The φ_{tract} was designed to incorporate WM axonal structural information to assess the damage to neural tracts. Current strain-based injury metrics, however, consider the aggregated measure of the injured volume. Therefore, we compared φ_{tract} with two additional injury susceptibility indices based on the total number of neural tract sampling points or traversing voxels, φ_{tract}^{point} and φ_{tract}^{voxel}, respectively. For all the three CC subregions regardless of the rotational direction, the two aggregated susceptibility indices were largely comparable between themselves (Fig. 10). This was not surprising, because they effectively sampled the same spatial domain (albeit, with different sampling resolutions). The two aggregated measures, however, were significantly lower than φ_{tract}, suggesting their potential underestimation of damage to neural tracts.

The current definition of φ_{tract} does not differentiate the relative susceptibility based on the number of sampling points with high ε_n^p exposure or the magnitude of ε_n^p along each fiber. A proper ''injury confidence'' weighting factor may be effective to further enhance

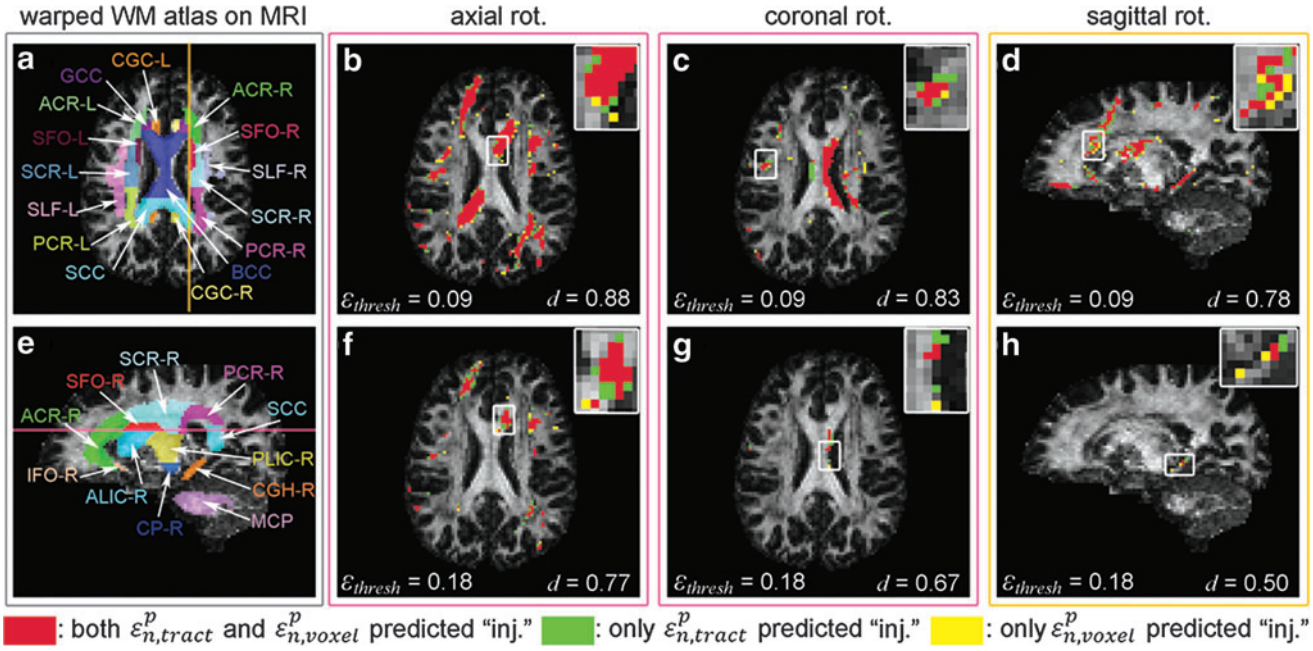

FIG. 7. The ICBM-81 white matter (WM) atlas warped onto the individual's anatomical magnetic resonance image (MRI) (**a** and **e**; on axial and sagittal MRI, respectively). Binary injury maps overlaid on an axial (for axial (**b** and **f**) and coronal (**c** and **g**) rotations) and a sagittal (for sagittal rotation; **d** and **h**) MRI. ''Injured'' voxels (i.e., corresponding to $\varepsilon^p_n > \varepsilon_{thresh}$) are color-coded depending on whether they were predicted by both or by only one of the strain evaluation techniques. For each MRI shown, the corresponding Dice coefficient, d, is reported. ($\varepsilon^p_{n,\,tract}$ and $\varepsilon^p_{n,\,voxel}$, refer to ε^p_n obtained from the tract- and voxel-based techniques, respectively). Color image is available online at www.liebertpub.com/neu

φ_{tract}. Regardless, the injury assessment utility of φ_{tract} that incorporates WM axonal structural information has not been employed before. This awaits further exploration.

WM injury directional dependency

Numerous model-based[30,32,58] and animal[59–61] injury studies have reported injury directional dependency. Our results were largely consistent with previous findings based on ε^p_{ep}, regardless of the strain evaluation technique. The axial rotation produced the largest extent of injury for the whole-brain WM (Table 2), which was consistent with previous reports based on ε^p_n,[21] regional average ε^p_{ep},[32] or CSDM.[31] The axial rotation also led to the largest tract-specific φ_{tract} in all three CC subregions (Fig. 9). The genu and splenium generally had a larger injury susceptibility than the main body in this rotation.

In the coronal rotation, the main body had the largest injury susceptibility. Contrary to earlier reports based on ε^p_{ep},[30,32] however, this rotation did not result in the largest damage to the CC anatomy (Table 2). Besides the different strain measures and kinematic inputs used, the discrepancy may be attributable to differences in the CC anatomy employed (ICBM atlas[45] here vs. FreeSurfer segmentation[22]; these give CC volume of 34.7 cm^3 and lateral width of 34 mm vs. 10.5 cm^3 and 12 mm, respectively).

While no injury was predicted in the CC anatomy in the sagittal rotation at the optimal ε_{thresh} (Table 2), a nonzero tract-specific φ_{tract} of 8.3% was observed for the CC main body (Fig. 9). This difference highlighted an important distinction between the voxel-wise and tract-specific injury susceptibility indices. The former measures local structural integrity by counting injured sampling points *within* the voxel or ROI. In contrast, the latter assesses global functional damage by counting injured fibers *regardless* of whether

TABLE 1. COMPARISON OF PREDICTED DISTRIBUTIONS OF POTENTIAL ''INJURY'' LOCATIONS IN TERMS OF DICE COEFFICIENT, D, BETWEEN THE VOXEL- AND TRACTOGRAPHY-BASED APPROACHES AT TWO ε_{thresh} LEVELS

ε_{thresh}			*Axial*	*Coronal*	*Sagittal*	Avg.
0.09		Dice coefficient, d	0.86	0.81	0.76	0.81
	FA	Both predicted ''injury''	0.51 ± 0.16 (8.6 k)	0.51 ± 0.18 (3.0 k)	0.48 ± 0.15 (3.2 k)	0.50
		Only one predicted ''injury''	0.34 ± 0.16 (2.7 k)	0.40 ± 0.16 (1.4 k)	0.41 ± 0.15 (2.0 k)	0.38
0.18		Dice coefficient, d	0.74	0.62	0.63	0.66
	FA	Both predicted ''injury''	0.51 ± 0.16 (1.7 k)	0.44 ± 0.22 (126)	0.40 ± 0.13 (83)	0.45
		Only one predicted ''injury''	0.42 ± 0.16 (1.2 k)	0.37 ± 0.16 (152)	0.33 ± 0.15 (96)	0.37

FA, fractional anisotropy.

Voxels consistently predicted as ''injured'' by the two approaches had a mean FA value significantly higher than those predicted by one but not the other. The numbers of identified voxels for each case are shown in parentheses.

Table 2. Summary of the Predicted Extent of Injury (as Percentages) for the Whole-Brain White Matter Voxels and the Three Corpus Callosum Subregions Using the Voxel- and Tractography-Based (in Parenthesis) Approaches at Two ε_{thresh} Levels

ε_{thresh}		*Axial %*	*Coronal %*	*Sagittal %*
0.09	Whole-brain	14.84 (16.05)	5.71 (5.99)	6.19 (6.61)
	Genu	35.53 (37.06)	1.53 (2.01)	2.20 (1.81)
	Main body	15.61 (16.85)	14.48 (15.31)	0.95 (0.59)
	Splenium	27.04 (28.72)	7.23 (7.48)	3.18 (2.55)
0.18	Whole-brain	2.95 (4.12)	0.29 (0.34)	0.15 (0.25)
	Genu	20.06 (23.30)	0 (0)	0 (0)
	Main body	3.56 (4.57)	0.83 (1.31)	0 (0)
	sSlenium	0.12 (0.37)	0 (0)	0 (0)

the injury occurred within or outside the corresponding anatomical boundary (Fig. 8).

Unlike a previous study that reported no injury in this rotation at the optimal threshold,[21] we also identified a small amount (0.2–0.3%) as potentially injured (Table 2). The discrepancy may have been the result of differences in simulated head impacts. In addition, the simplified 2D head models of [21], coupled with fiber direction projections that were unable to capture intrinsic 3D brain deformations (vs. a realistic 3D model with actual 3D fiber directions in our study), may also be responsible.

Finally, the directional dependency found with ε_n^p is also largely consistent with findings from an early monkey study.[59] The extent of DAI increased from sagittally to coronally rotated monkeys. Most axonal damage occurred in both cerebral hemispheres and the CC in axial and coronal rotations (all monkeys injured), while sagittal rotations only produced axonal damage in the cerebral hemispheres (in five of nine injured).

WM injury susceptibility

An important purpose of our study was to propose WM injury susceptibility indices to assess local structural integrity and functional damage to individual neural pathways (φ_{voxel} and φ_{tract}, respectively). Faithful and quantitative measurement of WM structural integrity at the voxel level may be important for direct correlation with longitudinal alterations in neuroimaging and with behavioral and cognitive measures in mild TBI, as suggested in numerous DTI studies (e.g., longitudinal changes in DTI parameters,[23,34,62] or WM abnormalities[63,64]). The voxel-wise susceptibility index may offer useful clinical insights and potentially serve as an important bridge among external head impacts, tissue-level mechanical responses, and neuroimaging, as previously attempted.[21,34]

Further, the tract-wise susceptibility index may also serve as a quantitative indicator for the relative vulnerabilities of WM neural

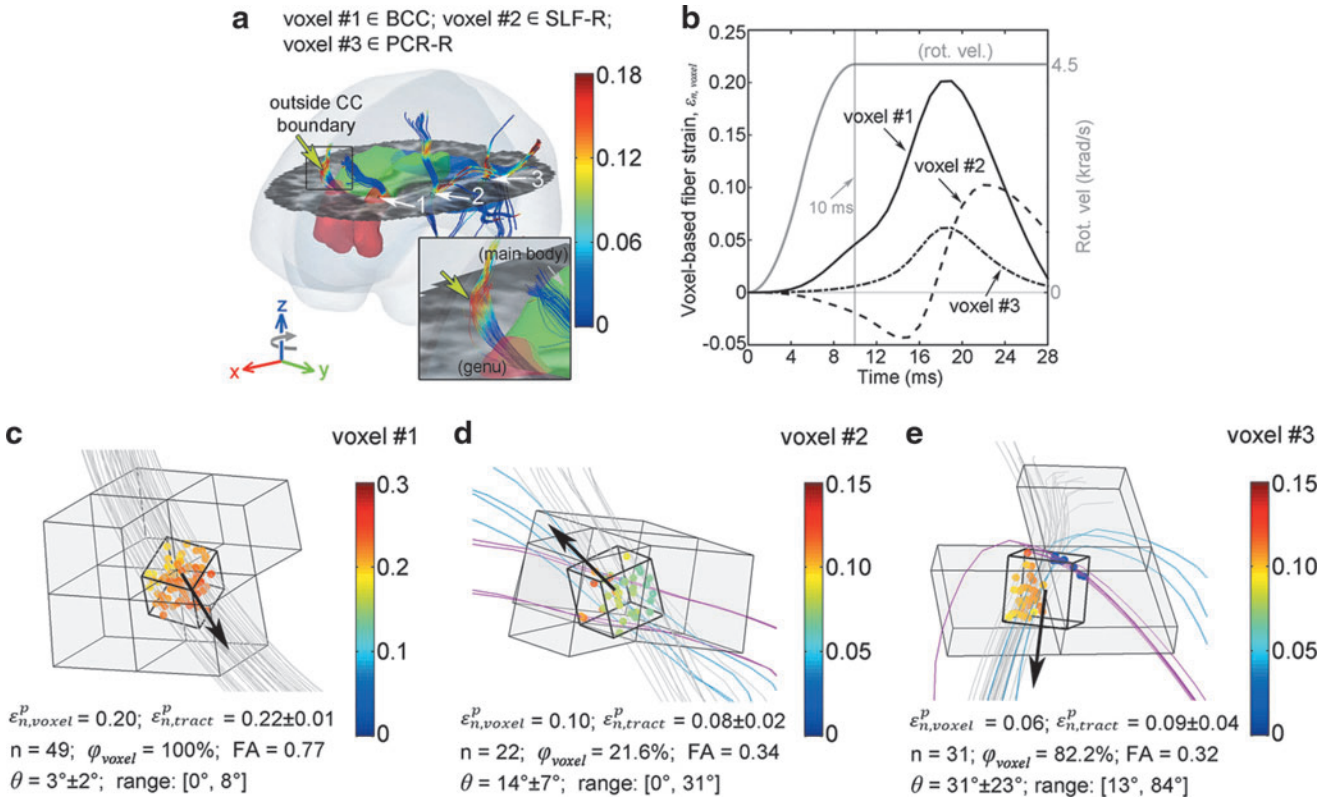

FIG. 8. Illustration of ε_n^p responses of intravoxel sampling points in three voxels. Intravoxel fiber sampling points are color-coded by ε_n^p from the tractography-based approach ($\varepsilon^p_{n,tract}$) using strain tensors from their nearest elements, as shown. *n*, number of intravoxel fibers, which was 45 ± 35 on average (range 0–269) for whole-brain white matter voxels; θ, angle between each fiber and the voxel-based average fiber orientation (arrows in b–d). All results based on ε_{thresh} of 0.09. (**a**) Voxel locations. (**b**) Time histories of $\varepsilon_{n,voxel}$ for the three identified voxels. (**c**) Both the voxel- and tractography-based approaches predicted potential ''injury'' for voxel #1. (**d**) The voxel-, but not the tractography-based, method predicted ''injury'' for voxel #2. (**e**) Vice versa for voxel #3. CC, corpus callosum. Color image is available online at www.liebertpub.com/neu

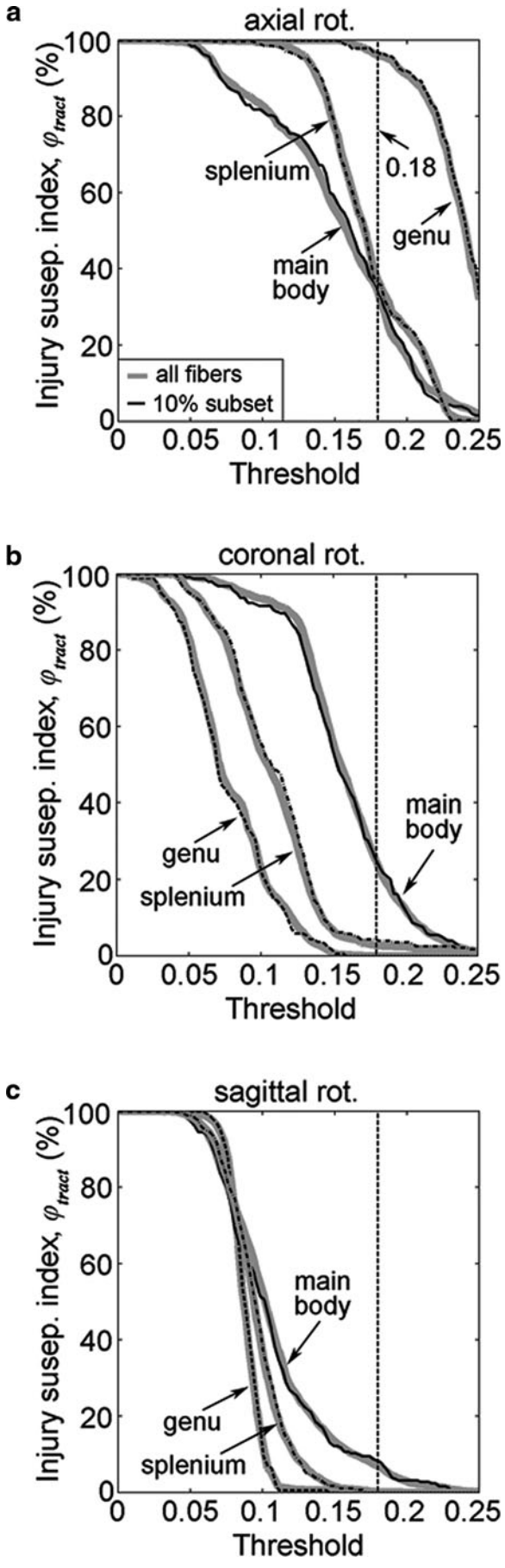

pathways. For example, because injury is assumed whenever high fiber strain occurred anywhere along an entire fiber length, regardless of the location, the tract-specific φ_{tract} implies longer tracts will be more prone to injury (notwithstanding potential difference in strain distributions between long and short tracts, or differences in injury tolerance). Indeed, this finding is consistent with neuropathological and DTI studies[65] that report long tracts—for example, frontal and temporal association WM tracts—are more susceptible to injury in mild TBI[62,66] and in moderate to severe brain injuries.[67] Therefore, we anticipate that the tractography-based ε_n^p evaluation technique and injury susceptibility measure developed here in the context of sports-related concussion or mild TBI may also be applicable to other, more severe strain-induced WM injuries.

Limitations

Several limitations must be noted. First, while we have focused our effort here on developing a tractography-based fiber strain evaluation technique and compared it with a previous voxel-based counterpart, we did not use real-world injury cases to discern their potential differences in injury prediction performance. On the voxel-level, the two approaches appear to differ primarily in predicting WM injury location and spatial distribution (Fig. 7 and Table 1), rather than the extent or binary injury status of the whole brain, according to results from the three idealized head impacts (Table 2). Therefore, real-world injury/noninjury cases with neuroimaging available (as opposed to injured vs. noninjured status only)[11,68] may be necessary to serve as an independent source of voxel-wise injury markers to correlate injuries with biomechanical findings.

Further investigations are needed to confirm the importance of a tractography-based approach and to verify the clinical significance of the WM injury susceptibility measures we established. These points will be the focus of future studies.

Second, there are limitations related to the neuroimaging data and tractography techniques currently available. Our tractography-based strain evaluation was based on ExploreDTI-generated tractography; however, it has been shown that different software packages can produce discordant results.[69] Therefore, there is some uncertainty about the accuracy of tractography-based results, and there is a need to better understand the impact of tractography software packages and/or techniques/parameters on ε_n^p and the resulting injury susceptibilities, which is beyond the scope of our current study.

In addition, fibers from tractography are still much larger in dimension than axons, and they do not incorporate features such as neuronal plasticity or dynamic ''rewiring'' on injury[29] that could be important to brain function as well. Regardless, we anticipate that our technique could be easily adapted when more advanced neuroimaging and/or more accurate tractography becomes available in the future.

Third, although our fiber sampling points were of high resolution (1 mm; generated from isotropic 2 mm DTI voxels), the DHIM mesh is still relatively coarse (average element size of 3.3 ± 0.79 mm;

FIG. 9. Tract-wise injury susceptibility index, φ_{tract}, as a function of ε_{thresh} for each corpus callosum (CC) subregion in (**a**) axial, (**b**) coronal, and (**c**) sagittal rotations. The results from the same 10% subset were virtually identical to those from the full set. At the ''optimal'' ε_{thresh} of 0.18, the largest φ_{tract} of 96.8% was observed for the genu in the axial rotation. The largest values of 25.3% and 8.3% occurred in the CC main body with coronal and sagittal rotations, respectively.

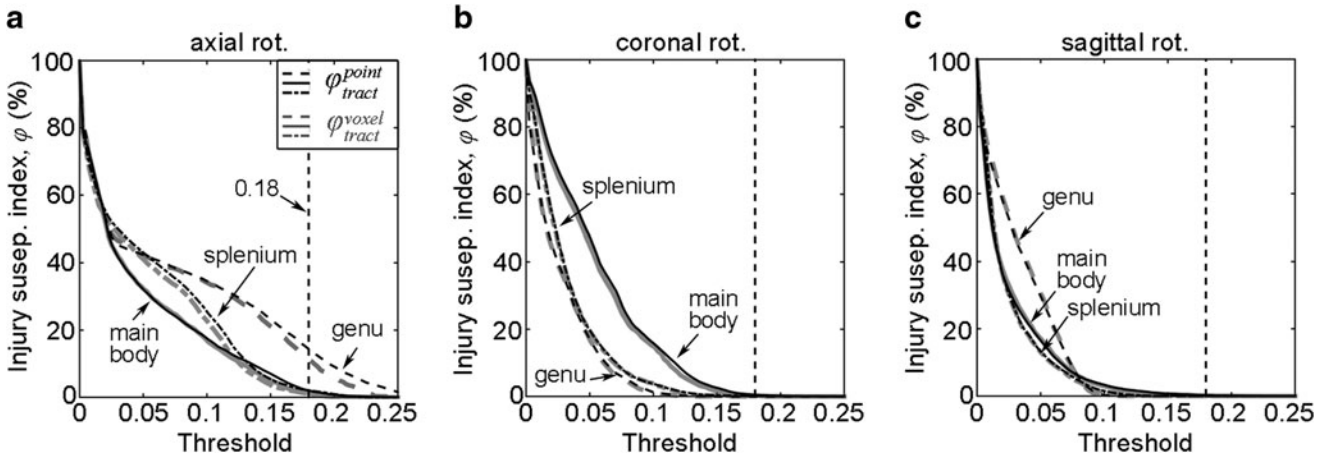

FIG. 10. Injury susceptibility indices, φ_{tract}^{point} and φ_{tract}^{voxel}, as a function of ε_{thresh} in (**a**) axial, (**b**) coronal, and (**c**) sagittal rotations. For each corpus callosum subregion, φ_{tract}^{point} and φ_{tract}^{voxel} were largely similar, but were significantly lower than the corresponding φ_{tract} (Fig. 9). At the ''optimal'' ε_{thresh}, the largest φ_{tract}^{point} and φ_{tract}^{voxel} were 14.6% and 11.5% in the genu in the axial rotation, respectively, and were virtually zero for the other two rotations.

total number of 55.1 k). Because a nearest neighbor interpolation was adopted,[22] the same strain tensor was used for all fiber sampling points within an element. Some resolution loss in ε_n^p spatial distribution is possible (Fig. 8). This limitation because of data discretization is common and well recognized in medical imaging.

Conceptually, the same limitation applies equally to other studies that incorporate averaged fiber orientations derived from uniformly sized DTI voxels into (even coarser) FE elements that typically have a range of sizes across the brain with differing local orientations. For example, Sahoo and associates[26] used isotropic 1 mm DTI voxels and 5320 brain elements of size 1.14–7.73 mm. In comparison, the KTH model coupled voxels of size 2 mm × 2 mm × 3.6 mm with 7128 brain elements, whose information on FE element size appears not available (albeit, anticipated to be comparable to the earlier example).[27]

To mitigate this issue, a multiscale simulation approach—already performed in brain injury analysis[17,19]—can be employed. This is analogous to the ''multiresolution'' strategy widely adopted in medical image registration. In this case, our relatively coarse FE mesh (compared with the 1 mm fiber sampling points) could serve as an initial estimation of whole-brain responses, from which more targeted, potentially injured, regions can be localized. A second level simulation with locally refined mesh resolution can then be employed to potentially improve accuracy.[11] Such a multiscale simulation strategy may offer an excellent compromise between accuracy and runtime. In addition, WM material anisotropy can also be incorporated at the microscale using explicit mesh representations, thereby avoiding the limitations in current studies that use rather coarse elements, as similarly envisioned.[11]

A fourth limitation is that the injury susceptibility only incorporates strain and not strain rate, which could also be important.[70] In addition, there may be regional differences in injury tolerance[71] that were not considered. We anticipate, however, that our injury susceptibility indices could be extended to combine both strain and strain rate (i.e., resulting in a function dependent on both variables) and further incorporate regional injury thresholds when they become available for injury definition.

Fifth, our tract-specific injury analysis was only applied to three CC subregions as an illustration. Nevertheless, we anticipate that the technique could be extended to other neural pathways (as many as 130 according to some investigators[72]). The significant additional computational time (~28 min for the three transcallosal tracts, which is expected to scale with the number of tracts considered) could be a concern. This may be mitigated by tract downsampling (e.g., using a 10% subset) to greatly reduce calculation time without significantly altering the results (Fig. 9). In addition, a pre-computation strategy may also be effective in the context of contact sports,[32,46] because the head's impact temporal characteristics appear largely similar within or across subjects.[50,51] On the other hand, when using realistic head impacts as model inputs, tract-specific injury susceptibility indices could allow assessment of the relative injury vulnerabilities of neural pathways to identify the most vulnerable ones in real-world injury scenarios. These will be the subjects of future investigations.

Last, similarly to other works evaluating fiber strain,[19,73] the DHIM uses a homogenous, isotropic material model for the entire brain. It does not yet incorporate material property heterogeneity[74] or WM material anisotropy (vs. structural anisotropy) resulting from fiber reinforcement.[26,27] While more sophisticated material properties for the brain may further enhance the model predictive power, we chose not to incorporate them in our current work for several practical reasons.

First, the fiber strain magnitude appears to be dominated by WM structural anisotropy rather than material anisotropy,[54] suggesting that focusing on the former via tractography is appropriate for our current ''technique development'' study. Second, although the baseline DHIM is subject-specific, we intend to use it for population-based studies as well—e.g., via the pre-computed brain response atlas (pcBRA[32,46,76]). Unfortunately, a detailed population-based, ''average'' DTI or tractography atlas appears unavailable, and it is not feasible to create a subject-specific pcBRA for each athlete (e.g., hundreds), at least at present.

If material anisotropy is incorporated using DTI from a single specific person (e.g., as in the baseline DHIM) while incorporating structural anisotropy from different athletes' respective DTI/tractography, there could be unwanted challenges in result interpretation because of the mismatch between the baseline model material anisotropy and individualized structural anisotropy. Employing a homogeneous material for the brain, although it may not be ideal, avoids such difficulties, and appears appropriate. On the other hand,

for individualized injury analyses (vs. population-based studies), incorporating WM material anisotropy may indeed be desirable. This appears relatively straightforward (e.g., via an existing Holzapfel-Gasser-Ogden model[75] in Abaqus[37]); nevertheless, it requires fresh model validations.[26,27] Given these considerations, it seems appropriate to incorporate DHIM with material anisotropy in a separate study in the future when suitable.

Regardless, incorporating transversely isotropic behavior for the WM may lower ε_n^p.[54] This is unlikely to significantly alter the relative magnitudes of the different WM injury susceptibility indices we established, however. On the other hand, it must be recognized that brain material properties represent only a narrow subset of the many variables important to predict injury (others include, e.g., injury tolerances, on-field impacts, neuroimaging, and clinical diagnosis of concussion, etc.). Given their uncertainty and potential errors, a systems approach may be necessary to yield a multifaceted understanding of the biomechanical mechanisms of TBI.[22]

Conclusion

We have developed a tractography-based approach for fiber strain evaluation using voxel- or anatomically constrained whole-brain tractography. The technique potentially improves previous element-/voxel-based techniques because it evaluates strains along the entire lengths of fibers (as opposed to averages on coarse elements/voxels). In addition, this technique enables quantifying the ''degree'' of local WM structural integrity and injury susceptibilities of functionally important neural pathways, which are not possible with previous methods. Therefore, the tractography-based approach may be important to enable new brain injury analyses in the future.

Voxel- and tract-wise injury susceptibility indices were also established to assess local WM structural integrity and functional damage in neural pathways. Implications from the tract-wise injury susceptibility measure were consistent with previous neuropathological and DTI studies of TBI across a spectrum of injury severities. Potentially, therefore, our study may lay important foundations for follow-on investigations using real-world head impacts and actual brain injury/noninjury cases to explore the multifaceted mechanisms of DAI.

Future investigations will: (1) analyze real-world impacts to confirm the importance of the tractography-based approach and to verify the clinical significance of the WM injury susceptibility measures; (2) apply the technique to other WM neural pathways; and (3) use realistic head impacts to assess the relative injury susceptibilities of WM neural pathways and identify the most vulnerable ones in real-world injury scenarios.

Acknowledgments

Funding is provided by the NIH grants R01 NS092853, R21 NS088781 and R21 NS078607, and the Dartmouth Hitchcock Foundation (SJ). JF was supported, in part, by The Dartmouth Clinical and Translational Science Institute, under award number UL1TR001086 from the National Center for Advancing Translational Sciences (NCATS) of the NIH. The content is solely the responsibility of the author(s) and does not necessarily represent the official views of the NIH.

SJ conceived and designed the study, drafted the manuscript; WZ carried out the work, created the contents, and participated in article drafting; JF generated tractography; JF, LF, and TM offered critical insight on neuroimaging and neuropathology; TM provided neuroimaging necessary for the work. All authors discussed the study, revised the article, and gave final approval for its publication.

Author Disclosure Statement

No competing financial interests exist.

References

1. CDC. (2013). Report to Congress on Traumatic Brain Injury in the United States: Understanding the Public Health Problem among Current and Former Military Personnel. Available at: www.cdc.gov. Accesed: February 26, 2016.
2. Versace, J. (1971). A review of the severity index, in: *15th Stapp Car Crash Conference*. Coronado, CA, pp. SAE paper 710881.
3. Kimpara, H., and Iwamoto, M. (2012). Mild traumatic brain injury predictors based on angular accelerations during impacts. Ann. Biomed. Eng. 40, 114–126.
4. Takhounts, E.G., Craig, M.J., Moorhouse, K., McFadden, J., and Hasija, V. (2013). Development of brain injury criteria (BrIC). Stapp Car Crash J. 57, 243–266.
5. Newman, J. (1986). A generalized acceleration model for brain injury threshold (GAMBIT)., in: *International IRCOBI Conference on the Biomechanics of Impact*. Zurich, Switzerland, pps. 121–131.
6. Newman, J., Shewchenko, N., and Welbourne, E. (2000). A proposed new biomechanical head injury assessment function—the maximum power index. Stapp Car Crash J. 44, 215–247.
7. Greenwald, R., Gwin, J., Chu, J., and Crisco, J. (2008). Head impact severity measures for evaluating mild traumatic brain injury risk exposure. Neurosurgery 62, 789–798.
8. Meaney, D.F., Morrison, B., and Bass, C.R. (2014). The mechanics of traumatic brain injury: a review of what we know and what we need to know for reducing its societal burden. J. Biomech. Eng. 136. AUTHOR: PLEASE UPPLY PAGE NUMBER.
9. Marjoux, D., Baumgartner, D., Deck, C., and Willinger, R. (2008). Head injury prediction capability of the HIC, HIP, SIMon and ULP criteria. Accid. Anal. Prev. 40, 1135–1148.
10. Hernandez, F., Wu, L.C., Yip, M.C., Hoffman, A.R., Lopez, J., Grant, G., Kleiven, S., and Camarillo, D.B. (2015). Six degree-of-freedom measurements of human mild traumatic brain injury. Ann. Biomed. Eng. 43, 1918–1934.
11. Giordano, C., and Kleiven, S. (2014). Evaluation of axonal strain as a predictor for mild traumatic brain injuries using finite element modeling. Stapp Car Crash J. 58, 29–61.
12. Holbourn, A.H. (1943). Mechanics of brain injuries. Lancet 2, 438–441.
13. Shuck, L.Z., and Advani, S.H. (1972). Rheological response of human brain tissue in shear. J. Basic Eng. 94, 905–911.
14. Bain, A.C., and Meaney, D.F. (2000). Tissue-level thresholds for axonal damage in an experimental model of central nervous system white matter injury. J. Biomech. Eng. 122, 615–622.
15. Morrison, B., III, Cullen, D., and LaPlaca, M. (2011). In vitro models for biomechanical studies of neural tissues. Neural Tissue Biomech. Stud. Mechanobiol. Tissue Eng. Biomater. 3, 247–285.
16. Cloots, R.J., van Dommelen, J.A., Nyberg, T., Kleiven, S., and Geers, M.G. (2011). Micromechanics of diffuse axonal injury: influence of axonal orientation and anisotropy. Biomech. Model. Mechanobiol. 10, 413–422.
17. Cloots, R.J., van Dommelen, J. A., Kleiven, S., and Geers, M.G. (2012). Multi-scale mechanics of traumatic brain injury: predicting axonal strains from head loads. Biomech. Model. Mechanobiol. 12, 137–150.
18. Chatelin, S., Deck, C., Renard, F., Kremer, S., Heinrich, C., Armspach, J.P., and Willinger, R. (2011). Computation of axonal elongation in head trauma finite element simulation. J. Mech. Behav. Biomed. Mater. 4, 1905–1919.
19. Wright, R.M., and Ramesh, K.T. (2012). An axonal strain injury criterion for traumatic brain injury. Biomech. Model. Mechanobiol. 11, 245–260.
20. Kraft, R.H., McKee, P.J., Dagro, A.M., and Grafton, S.T. (2012). Combining the finite element method with structural connectome-based analysis for modeling neurotrauma: connectome neurotrauma mechanics. PLoS Comput. Biol. 8, e1002619.

21. Wright, R.M., Post, A., Hoshizaki, B., and Ramesh, K.T. (2013). A multiscale computational approach to estimating axonal damage under inertial loading of the head. J. Neurotrauma 30, 102–118.
22. Ji, S., Zhao, W., Ford, J.C., Beckwith, J.G., Bolander, R.P., Greenwald, R.M., Flashman, L.A., Paulsen, K.D., and McAllister, T.W. (2015). Group-wise evaluation and comparison of white matter fiber strain and maximum principal strain in sports-related concussion. J. Neurotrauma 32, 441–454.
23. Bazarian, J.J., Zhu, T., Blyth, B., Borrino, A., and Zhong, J. (2012). Subject-specific changes in brain white matter on diffusion tensor imaging after sports-related concussion. Magn. Reson. Imaging 30, 171–180.
24. Takhounts, E.G., Eppinger, R.R., Campbell, J.Q., Tannous, R.R., Power, E., and Shook, L. (2003). On the development of the SIMon finite element head model. Stapp Car Crash J. 47, 107–133.
25. Carlsen, R.W., and Daphalapurkar, N.P. (2015). The importance of structural anisotropy in computational models of traumatic brain injury. Front. Neurol. 6, 28.
26. Sahoo, D., Deck, C., and Willinger, R. (2014). Development and validation of an advanced anisotropic visco-hyperelastic human brain FE model. J. Mech. Behav. Biomed. Mater. 33, 24–42.
27. Giordano, C., and Kleiven, S. (2014). Connecting fractional anisotropy from medical images with mechanical anisotropy of a hyperviscoelastic fibre-reinforced constitutive model for brain tissue. J. R. Soc. Interface 11, 20130914.
28. Roossien, D.H., Lamoureux, P., and Miller, K.E. (2014). Cytoplastmic dynein pushes the cytoskeletal meshwork forward during axonal elongation. J. Cell Sci. 127, 3593–3602.
29. Debanne, D., Campanac, E., Bialowas, A., Carlier, E., and Alcaraz, G. (2011). Axon physiology. Physiol. Rev. 91, 555–602.
30. Kleiven, S. (2006). Evaluation of head injury criteria using a finite element model validated against experiments on localized brain motion, intracerebral acceleration, and intracranial pressure. Int. J. Crashworthiness 11, 65–79.
31. Weaver, A.A., Danelson, K.A., and Stitzel, J.D. (2012). Modeling brain injury response for rotational velocities of varying directions and magnitudes. Ann. Biomed. Eng. 40, 2005–2018.
32. Zhao, W., and Ji, S. (2015). Parametric investigation of regional brain strain responses via a pre-computed atlas., in: *IRCOBI Conference*. Lyon, France, pps. 208–220.
33. McAllister, T.W., Ford, J.C., Flashman, L.A., Maerlender, A., Greenwald, R.M., Beckwith, J.G., Bolander, R.P., Tosteson, T.D., Turco, J.H., Raman, R., and Jain, S. (2014). Effect of head impacts on diffusivity measures in a cohort of collegiate contact sport athletes. Neurology 82, 63–69.
34. McAllister, T.W., Ford, J.C., Ji, S., Beckwith, J.G., Flashman, L.A., Paulsen, K., and Greenwald, R.M. (2012). Maximum principal strain and strain rate associated with concussion diagnosis correlates with changes in corpus callosum white matter indices. Ann. Biomed. Eng. 40, 127–140.
35. Zhao, W., Ruan, S., and Ji, S. (2015). Brain pressure responses in translational head impact: a dimensional analysis and a computational study. Biomech. Model. Mechanobiol. 14, 753–766.
36. Ji, S., Zhao, W., Li, Z., and McAllister, T.W. (2014). Head impact accelerations for brain strain-related responses in contact sports: a model-based investigation. Biomech. Model. Mechanobiol. 13, 1121–1136.
37. Abaqus. (2012). Abaqus Online Documentation, Abaqus 6.12.
38. Hardy, W.N., Mason, M.J., Foster, C.D., Shah, C.S., Kopacz, J.M., Yang, K.H., King, A.I., Bishop, J., Bey, M., Anderst, W., and Tashman, S. (2007). A study of the response of the human cadaver head to impact. Stapp Car Crash J. 51, 17–80.
39. Hardy, W.N., Foster, C.D., Mason, M.J., Yang, K.H., King, A.I., and Tashman, S. (2001). Investigation of head injury mechanisms using neutral density technology and high-speed biplanar x-ray. Stapp Car Crash J. 45, 337–68.
40. Nahum, A., Smith, R., and Ward, C. (1977). Intracranial pressure dynamics during head impact. SAE Tech. Pap., No. 770922.
41. Trosseille, X., Tarriere, C., Lavaste, F., Guillon, F., and Domont, A. (1992). Development of a FEM of the human head according to a specific test protocol., in: *Proceedings of 46th Stapp Car Conference*. pps. 235–253.
42. Sabet, A.A., Christoforou, E., Zatlin, B., Genin, G.M., and Bayly, P.V. (2008). Deformation of the human brain induced by mild angular head acceleration. J. Biomech. 41, 307–315.
43. Leemans, A., Jeurissen, B., Siibers, J., and Jones, D. (2009). ExploreDTI: a graphical tool box for processing, analyzing, and visualizing diffusion MR data., in: *17th Anuual Meeting of the International Society of Magnetic Resonance in Medicine*. Hawaii.
44. Prasad, G., Joshi, S.H., Jahanshad, N., Villalon-Reina, J., Aganj, I., Lenglet, C., Sapiro, G., McMahon, K.L., de Zubicaray, G.I., Martin, N.G., Wright, M.J., Toga, A.W., and Thompson, P.M. (2014). Automatic clustering and population analysis of white matter tracts using maximum density paths. Neuroimage 97, 284–295.
45. Mori, S., Oishi, K., Jiang, H., Jiang, L., Li, X., Akhter, K., Hua, K., Faria, A.V., Mahmood, A., Woods, R., Toga, A.W., Pike, G.B., Neto, P.R., Evans, A., Zhang, J., Huang, H., Miller, M.I., van Zijl, P., and Mazziotta, J. (2008). Stereotaxic white matter atlas based on diffusion tensor imaging in an ICBM template. Neuroimage 40, 570–582.
46. Ji, S., and Zhao, W. (2015). A pre-computed brain response atlas for instantaneous strain estimation in contact sports. Ann. Biomed. Eng. 43, 1877–1895.
47. Ji, S., Ghadyani, H., Bolander, R.P., Beckwith, J.G., Ford, J.C., McAllister, T.W., Flashman, L.A., Paulsen, K.D., Ernstrom, K., Jain, S., Raman, R., Zhang, L., and Greenwald, R.M. (2014). Parametric comparisons of intracranial mechanical responses from three validated finite element models of the human head. Ann. Biomed. Eng. 42, 11–24.
48. Rowson, S., Duma, S.M., Beckwith, J.G., Chu, J.J., Greenwald, R.M., Crisco, J.J., Brolinson, P.G., Duhaime, A.C., McAllister, T.W., and Maerlender, A.C. (2012). Rotational head kinematics in football impacts: an injury risk function for concussion. Ann. Biomed. Eng. 40, 1–13.
49. Broglio, S.P., Schnebel, B., Sosnoff, J.J., Shin, S., Fend, X., He, X., and Zimmerman, J. (2010). Biomechanical properties of concussions in high school football. Med. Sci. Sports Exerc. 42, 2064–2071.
50. Broglio, S.P., Sosnoff, J.J., Shin, S., He, X., Alcaraz, C., and Zimmerman, J. (2009). Head impacts during high school football: a biomechanical assessment. J. Athl. Train. 44, 342–349.
51. Camarillo, D.B., Shull, P.B., Mattson, J., Shultz, R., and Garza, D. (2013). An instrumented mouthguard for measuring linear and angular head impact kinematics in American football. Ann. Biomed. Eng. 41, 1939–1949.
52. Zhang, L., Yang, K.H., and King, A.I. (2004). A proposed injury threshold for mild traumatic brain injury. J. Biomech. Eng. 126, 226–236.
53. Kleiven, S. (2007). Predictors for traumatic brain injuries evaluated through accident reconstructions. Stapp Car Crash J. 51, 81–114.
54. Giordano, C., Cloots, R.J., van Dommelen, J.A., and Kleiven, S. (2014). The influence of anisotropy on brain injury prediction. J. Biomech. 47, 1052–1059.
55. Talavage, T.M., Nauman, E.A., Breedlove, E.L., Yoruk, U., Dye, A.E., Morigaki, K.E., Feuer, H., and Leverenz, L.J. (2013). Functionally-detected cognitive impairment in high school football players without clinically-diagnosed concussion. J. Neurotrauma 31, 327–338.
56. Bazarian, J.J., Zhu, T., Zhong, J., Janigro, D., Rozen, E., Roberts, A., Javien, H., Merchant-Borna, K., Abar, B., and Blackman, E.G. (2014). Persistent, long-term cerebral white matter changes after sports-related repetitive head impacts. PLoS One 9, e94734.
57. Bain, A.C., Shreiber, D.I., and Meaney, D.F. (2003). Modeling of microstructural kinematics during simple elongation of central nervous system tissue. J. Biomech. Eng. 125, 798–804.
58. Kleiven, S. (2003). Influence of impact direction on the human head in prediction of subdural hematoma. J. Neurotrauma 20, 365–379.
59. Gennarelli, T., Thibault, L., and Tomei, G. (1987). Directional dependence of axonal brain injury due to centroidal and non-centroidal acceleration.
60. Smith, D.H., Nonaka, M., Miller, R., Leoni, M., Chen, X.H., Alsop, D., and Meaney, D.F. (2000). Immediate coma following inertial brain injury dependent on axonal damage in the brainstem. J. Neurosurg. 93, 315–322.
61. Eucker, S.A., Smith, C., Ralston, J., Friess, S.H., and Margulies, S.S. (2011). Physiological and histopathological responses following closed rotational head injury depend on direction of head motion. Exp. Neurol. 227, 79–88.
62. Niogi, S.N., and Mukherjee, P. (2010). Diffusion tensor imaging of mild traumatic brain injury. J. Head Trauma Rehabil. 25, 241–255.
63. Lo, C., Shifteh, K., Gold, T., Bello, J.A., and Lipton, M.L. (2009). Diffusion tensor imaging abnormalities in patients with mild traumatic

brain injury and neurocognitive impairment. J. Comput. Assist. Tomogr. 33, 293–297.
64. Messé, A., Caplain, S., Paradot, G., Garrigue, D., Mineo, J.F., Soto Ares, G., Ducreux, D., Vignaud, F., Rozec, G., Desal, H., Pélégrini-Issac, M., Montreuil, M., Benali, H., and Lehéricy, S. (2011). Diffusion tensor imaging and white matter lesions at the subacute stage in mild traumatic brain injury with persistent neurobehavioral impairment. Hum. Brain Mapp. 32, 999–1011.
65. Bigler, E.D., and Maxwell, W.L. (2012). Neuropathology of mild traumatic brain injury: relationship to neuroimaging findings. Brain Imaging Behav. 6, 108–136.
66. Kraus, M.F., Susmaras, T., Caughlin, B.P., Walker, C.J., Sweeney, J.A., and Little, D.M. (2007). White matter integrity and cognition in chronic traumatic brain injury: a diffusion tensor imaging study. Brain 130, 2508–2519.
67. Greenberg, G., Mikulis, D.J., Ng, K., DeSouza, D., and Green, R.E. (2008). Use of diffusion tensor imaging to examine subacute white matter injury progression in moderate to severe traumatic brain injury. Arch. Phys. Med. Rehabil. 89, S45–S50.
68. Viano, D.C., Casson, I.R., Pellman, E.J., Zhang, L., King, A.I., and Yang, K.H. (2005). Concussion in professional football: Brain responses by finite element analysis–part 9. Neurosurgery 57, 891–916.
69. Feigl, G., Hiergeist, W., Fellner, C., Schebesch, K., Doenitz, C., Finkenzeller, T., Brawanski, A., and Schlaier, J. (2014). Magnetic resonance imaging diffusion tensor tractography: evaluation of anatomic accuracy of different fiber tracking software packages. World Neurosurg 81, 144–150.
70. Morrison, B., 3rd, Elkin, B.S., Dollé, J.P., and Yarmush, M.L. (2011). In vitro models of traumatic brain injury. Annu. Rev. Biomed. Eng. 13, 91–126.
71. Elkin, B.S., and Morrison, B. (2007). Region-specific tolerance criteria for the living brain. Stapp Car Crash J. 51, 127–138.
72. Zhang, Y., Zhang, J., Oishi, K., Faria, A.V., Jiang, H., Li, X., Akhter, K., Rosa-Neto, P., Pike, G.B., Evans, A., Toga, A.W., Woods, R., Mazziotta, J.C., Miller, M.I., van Zijl, P.C., and Mori, S. (2010). Atlas-guided tract reconstruction for automated and comprehensive examination of the white matter anatomy. Neuroimage 52, 1289–1301.
73. Sullivan, S., Eucker, S.A., Gabrieli, D., Bradfield, C., Coats, B., Maltese, M.R., Lee, J., Smith, C., and Margulies, S.S. (2014). White matter tract-oriented deformation predicts traumatic axonal brain injury and reveals rotational direction-specific vulnerabilities. Biomech. Model. Mechanobiol. 14, 877–896.
74. Van Dommelen, J.A., van der Sande, T.P., Hrapko, M., and Peters, G.W. (2010). Mechanical properties of brain tissue by indentation: interregional variation. J. Mech. Behav. Biomed. Mater. 3, 158–166.
75. Gasser, T., Ogden, R., and Holzapfel, G. (2006). Hyperelastic modelling of arterial layers with distributed collagen fibre orientations. J. R. Soc. Interface 3, 15–35.
76. Zhao W, and Ji, S. (2016). Real-time, whole-brain, temporally resolved pressure reponses translational head impact. Interface Focus 6.

Address correspondence to:
Songbai Ji, DSc
Thayer School of Engineering
Dartmouth College
14 Engineering Drive
Hanover, NH 03766

E-mail: Songbai.Ji@Dartmouth.edu